SCIENTIFIC HIGHLIGHTS

CONDENSED MATTER PHYSICS

The main objectives of research in the framework of the theme involved the application of neutron scattering techniques and complementary methods to investigate the structure, dynamics and microscopic properties of nanosystems and novel materials, which are of great importance for the development of nanotechnologies in the fields of electronics, pharmacology, medicine, chemistry, modern condensed matter physics and interdisciplinary sciences.

The greater part of experimental research was carried out on the spectrometers of the modernized IBR-2 reactor in accordance with the Topical Plan for JINR Research and International Cooperation and FLNP User Program. A number of scientific experiments were performed in neutron and synchrotron centers in Russia and abroad under the existing cooperation agreements and accepted beam time application proposals. Also, the activities on the modernization of the available spectrometers and the development of new instruments were carried out in accordance with the development program plan for the IBR-2 spectrometers.

Within the framework of investigations under the theme the employees of the FLNP Department of Neutron Investigations of Condensed Matter (NICM) maintained broad cooperation with many scientific organizations in Russia and abroad. The cooperation, as a rule, was documented by joint protocols or agreements. In Russia, especially active collaboration was with the thematically-close organizations, such as RRC KI, PNPI, MSU, IMP UB RAS, IC RAS, INR RAS and others.

A list of the main scientific topics studied by the employees of the NICM Department includes:

- Investigation of the structure and properties of novel functional materials;
- Investigation of the structure and properties of materials under extreme conditions;
- Investigation of fundamental regularities of real-time processes in condensed matter;
- Investigation of atomic dynamics of materials for nuclear power engineering;
- Computer simulation of physical and chemical properties of novel crystalline and nanostructured materials;
- Investigation of magnetic properties of layered nanostructures;
- Investigation of structural characteristics of carbon- and silicon-containing nanomaterials;
- Investigation of molecular dynamics of nanomaterials;
- Investigation of magnetic colloidal systems in bulk and at interfaces;
- Structural analysis of polymer nanodispersed materials;
- Investigation of supramolecular structure and functional characteristics of biological materials;
- Investigation of structure and properties of lipid membranes and lipid complexes;
- Investigation of texture and physical properties of Earth's rocks, minerals and engineering materials;
- Non-destructive control of internal stresses in industrial products and engineering materials;
- Introscopy of internal structure and processes in industrial products, rocks and natural heritage objects.

Structure investigations of novel oxide, intermetallic and nanostructured materials

Binary copper oxide CuO is one of the most structurally simple improper multiferroics in which spontaneous ferroelectric polarization arises as a result of symmetry inversion violation by the modulated antiferromagnetic (AFM) ordering formed in the intermediate phase in the temperature range T_{N1} - T_N 213-230 K. Theoretical calculations predicted the existence of such a phase at room temperature at high pressures of 20-40 GPa and the extension of its temperature range up to 0 K. To verify this assumption, the atomic and magnetic structures of CuO were studied by neutron and X-ray diffraction, **Fig. I-1-1** [1]. It was revealed that the crystal lattice compressibility of the monoclinic CuO structure exibits an anomalous behavior; it is accompanied first by an increase in the lattice parameter *a* in the pressure range of up to 13 GPa, and then by its decrease (with a subsequent growth in pressure up to 40 GPa) down to the value approximately equal to the value at normal pressure. No anomalies in the behavior of other lattice parameters were observed. The Néel temperature in the pressure range of up to 11 GPa increases up to 250 K. The region of existence of the incommensurate AFM phase with ferroelectric polarization at high pressures was determined using temperature dependences of the monoclinic angle of the crystal lattice for which the anomalies at the points of magnetic transitions, T_N and T_{N1}, are observed (**Fig. I-1-1**). The temperature range of its stability extends under pressure.

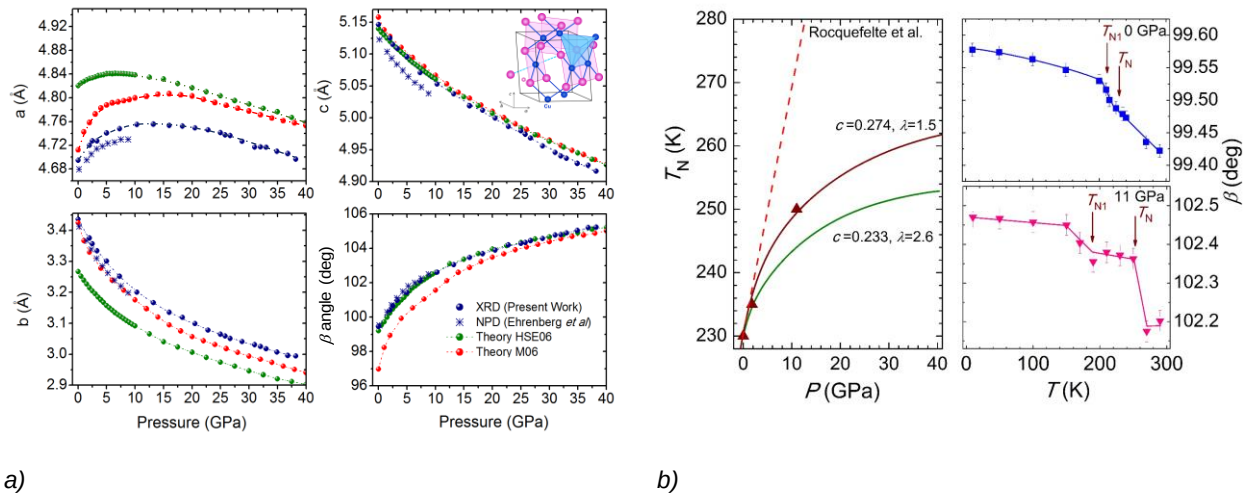

a) *b)*

Fig. I-1-1. *Pressure dependences of unit cell parameters of CuO (a). Experimental points, results of theoretical DFT calculations using hybrid functionals HSE06, M06 and results of previous neutron studies are shown. Experimental and calculated pressure dependences of Néel temperature and temperature dependences of monoclinic angle of CuO crystal lattice at a pressure of 0 and 11 GPa (b).*

The estimates based on the experimental data showed that at a pressure range of up to 40 GPa the Néel temperature increases up to about 265 K, which is much below room temperature. To explain the observed anomalies in the structural behavior of CuO under pressure, theoretical first principles calculations were carried out and successfully reproduced the pressure dependences for the structural parameters.

SCIENTIFIC HIGHLIGHTS

Another simple binary oxide, Cr_2O_3 (escoilite), is one of the first known magnetoelectric materials, in which the occurrence of spontaneous ferroelectric polarization under external magnetic fields was found. In the previous high-pressure studies of Cr_2O_3 by second harmonic optical spectroscopy, it was suggested that a magnetic phase transition occurs at P ~ 20 GPa, which can result in the suppression of the magnetoelectric effect. The stability of the initial magnetic structure and the absence of magnetic phase transitions at pressures up to 35 GPa were established in the neutron diffraction studies of Cr_2O_3 [2] performed in the temperature range of 4-300 K at the DN-6 diffractometer, **Fig. I-1-2**. At the same time, the Néel temperature (T_N = 307 K at P = 0) rises under compression with the positive pressure coefficient dT_N/dP = 2.8 K/GPa.

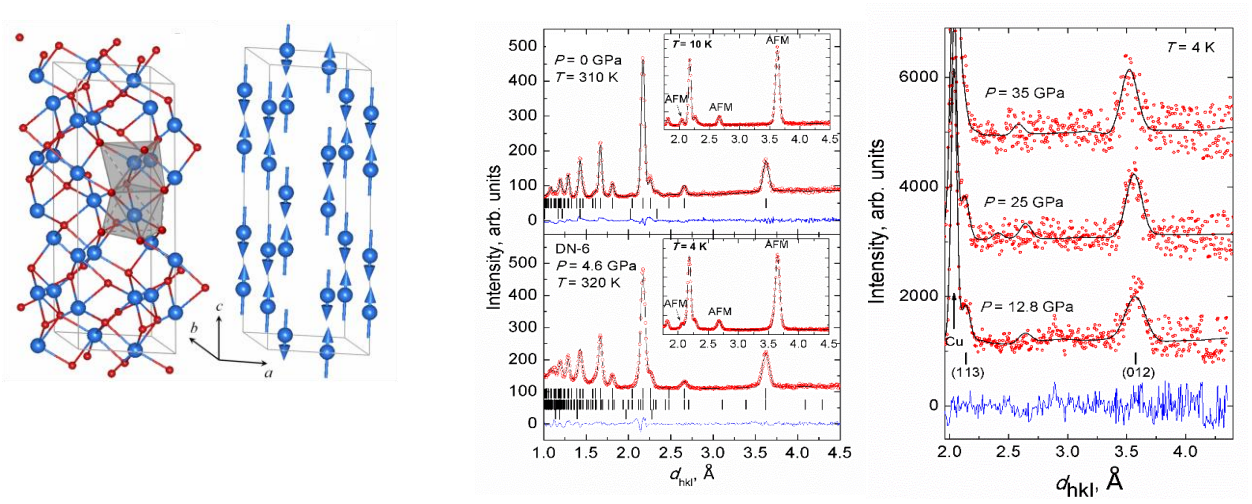

a) *b)*

Fig. I-1-2. *Rhombohedral crystal structure with R$\bar{3}$c symmetry and AFM structure of Cr_2O_3 (a). Neutron diffraction spectra of Cr_2O_3 at various temperatures and pressures in the range of up to 35 GPa refined by the Rietveld method (b).*

An anomalous structural phase separation observed in layered electrode materials of lithium-ion batteries at first charging and disappearing during their subsequent operation, was investigated. The study was carried out for $Li_xNi_{0.8}Co_{0.15}Al_{0.05}O_2$ (NCA) prepared at different calendering levels (high-temperature rolling to reduce electrode bulk density). A specialized electrochemical cell with a new design was used in the neutron experiment. The in operando/in situ studies were performed at the HRFD diffractometer. The presented illustrations (**Fig. I-1-3**) clearly show a splitting of the diffraction peak (003) because of the formation of a two-phase state in the cathode material. The analysis of the obtained results revealed [3] that the phase-separation state in NCA in the first electrochemical cycle observed by diffraction is not caused by the properties of atomic and electronic structures of NCA but determined by the peculiarities of the microstructure of material in use.

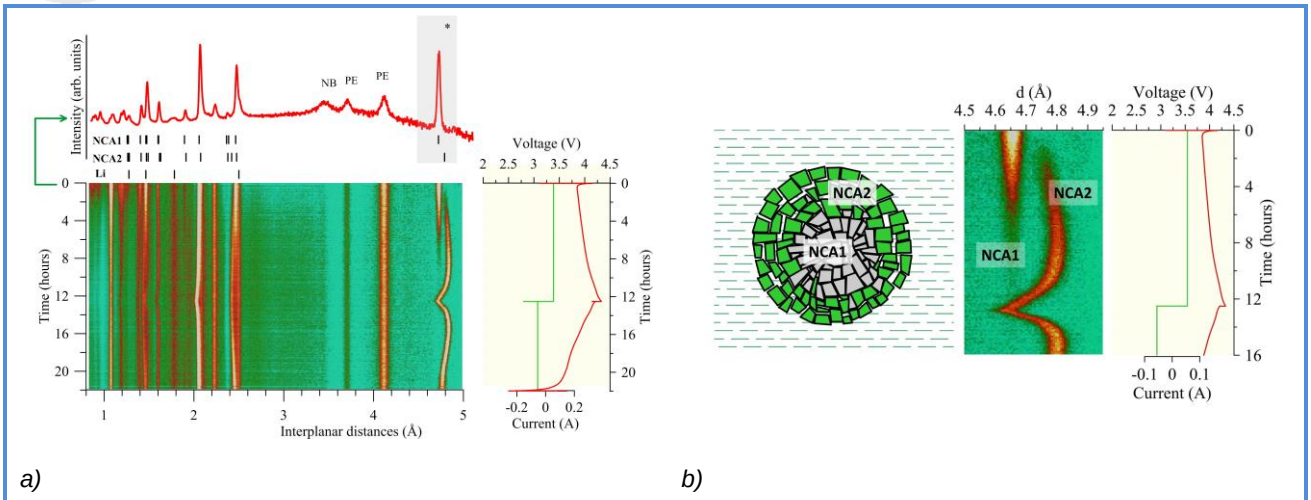

a) b)

Fig. I-1-3. *(a) Evolution of diffraction peaks from NCA electrode material during electrochemical cycling. Measurements were made with a specialized electrochemical cell. At the top, diffraction spectrum for the initial state of NCA is given. In addition to the peaks from anode and cathode, peaks from boron nitride (NB) and a separator (PE) can be seen. The asterisk denotes the area of peak (003) from NCA, which was used in the analysis of the phase separation, manifesting as a splitting at a certain level of charge. (b) Evolution of peak 003 from NCA material during first charging. Model representation of the process shows a spherical conglomerate of primary NCA particles during electrochemical cycling. The gray area corresponds to the NCA1 phase which does not satisfactory contact with electrolyte. The green-colored particles correspond to the NCA2 phase already in contact with electrolyte (at the left).*

Iron manganese alloys are well known as functional materials exhibiting the shape-memory effect and possessing high internal friction and other interesting physical properties. Despite the fact that the mechanism of the shape-memory effect in these alloys, which is based on the martensitic transformation fcc ↔ hcp (γ ↔ ε), is generally well studied, there remain unanswered questions related to the influence of preliminary heat treatment of the alloy on its microstructure, temperature and kinetics of structural transitions. To clarify these questions, a martensitic transition in two samples with composition Fe-22% Mn-3% Si was studied by neutron diffraction [4]. The two samples were subjected to a different number of heating-cooling cycles, namely the first sample (S1) underwent 1 cycle and the second sample (S12) – 12 cycles. The measurements were carried out at the HRFD diffractometer in two modes (high intensity and high resolution). Diffraction spectra during heating-cooling cycles (rate of temperature change of about 2 K/min) were measured in situ with an exposure time ts = 1 min, which made it possible to analyze the kinetics of structural transitions and accompanying effects. The microstructural parameters were obtained from the diffraction spectra measured with high resolution (Δd/d ≈ 0.002). In both samples, there was a mixture of phases A1 (γ, fcc, sp. gr. Fm3m; a ≈ 3.693 Å) and A3 (ε, hcp, sp. gr. P63/mmc; a ≈ 2.534 Å, c ≈ 4.103 Å) (**Fig. I-1-4**). The amount of phase A3 in sample S2 was several times greater than in sample S1, which is evident from the ratio of intensities of peaks (002)A3 and (111)A1. When heating, the structural transition occurred at about 200°C, which can be seen from the behavior of intensities of characteristic diffraction peaks (**Fig. I-1-4**). In sample S1, the transition A1 + A3 → A1 was completed at T ≈ 190°C, whereas in sample S12 it occurred at T ≈ 220°C. When cooling, the transition A1 → A1 + A3 occurred at T ≈ 120°C and T ≈ 100°C for S1 and S12, respectively. These temperatures of the reversible non-diffusion transition ε ↔ γ are in

good agreement with the data obtained by other methods (DSC and TDIF). The comparison of the phase transition kinetics in the samples under study has shown that the shift in the transition temperature in S1 and S12 (defined as the temperature at which the fraction of phase A3 decreases by a factor of two) is about 34°C. In addition, the transition kinetics in S12 is somewhat slower than in S1.

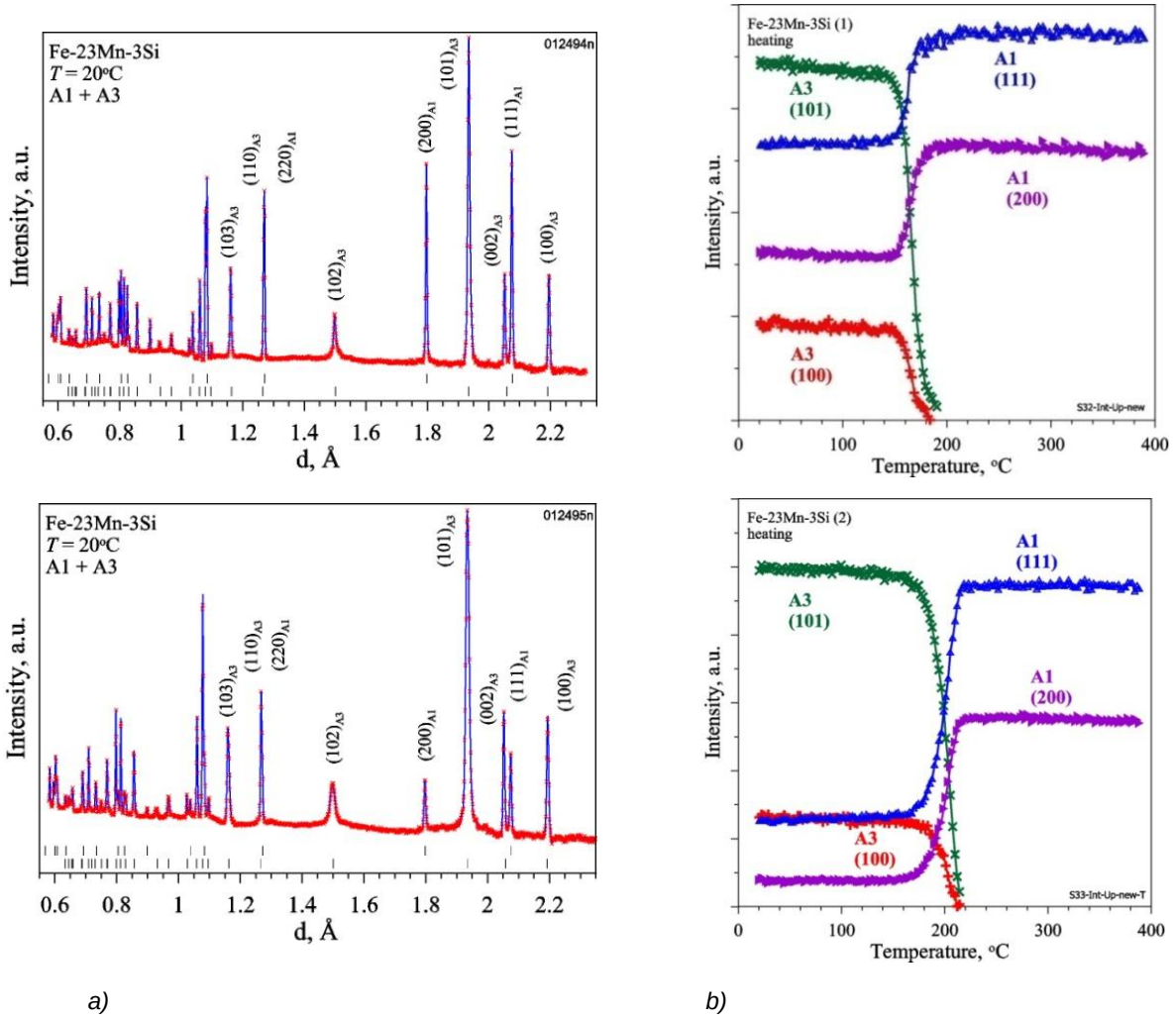

a) *b)*

Fig. I-1-4. *(a) Neutron diffraction spectra of samples S1 (top) and S12 (bottom) in the initial state. All peaks correspond to either phase A1 (Fm3m) or phase A3 (P63/mmc). (b) Temperature dependences for intensities of characteristic diffraction peaks for A1 and A3 phases in samples S1 (top) and S12 (bottom).*

Catalytic materials (copper-containing spinel oxides CuB_2O_4 ($B = Me^{3+}$) were studied. One of the effective methods for regulating physicochemical properties and controlled synthesis of spinels with defined properties is a variation of chemical composition and ratio of components. The structural characteristics of nanodispersed powders of spinels $CuFe_{2-x}Cr_xO_4$ ($x = 0 \div 2$) were determined by neutron diffraction. The interval of Fe/Cr ratio that ensures the existence of cubic and tetragonal spinel modifications was refined. The cation distribution between octa- and

tetrahedral positions was estimated. A correlation was found between the distribution of catalytically active Cu^{2+} cations in the spinel structure and the activation energy of the low-temperature CO vapour conversion reaction. The variation of the chemical nature and ratio of Me^{3+} cations make it possible to regulate the activation energy of the model catalytic reaction of CO vapour conversion, which is an important energy characteristic of copper as a catalytically active component of catalysts.

Investigation of magnetic fluids and nanoparticles

The structural organization of layers of gold nanoparticles deposited from aqueous solutions on silicon substrate and functionalized with a molecular layer of 1.9-nonanedithiol (promising systems for nanoelectronic devices due to their specific optical properties) was studied. For a full description of the system, data of neutron reflectometry, atomic force microscopy, X-ray reflectometry and diffraction were used. On the basis of neutron reflectometry data (GRAINS reflectometer) the structure profile of gold nanoparticle layers was determined and used to estimate the layer thickness and particle packing density (**Fig. I-1-5**). The presence of water molecules in the adsorbed layers of gold nanoparticles was established. The obtained results were used in the complex approach, which allowed us to reliably and unambiguously describe the surface packing of nanoparticles [5]. The study was performed in cooperation with the Chuiko Institute of Surface Chemistry NASU, Institute of Physics NASU, Faculty of Physics of Taras Shevchenko National University of Kyiv (Kiev, Ukraine).

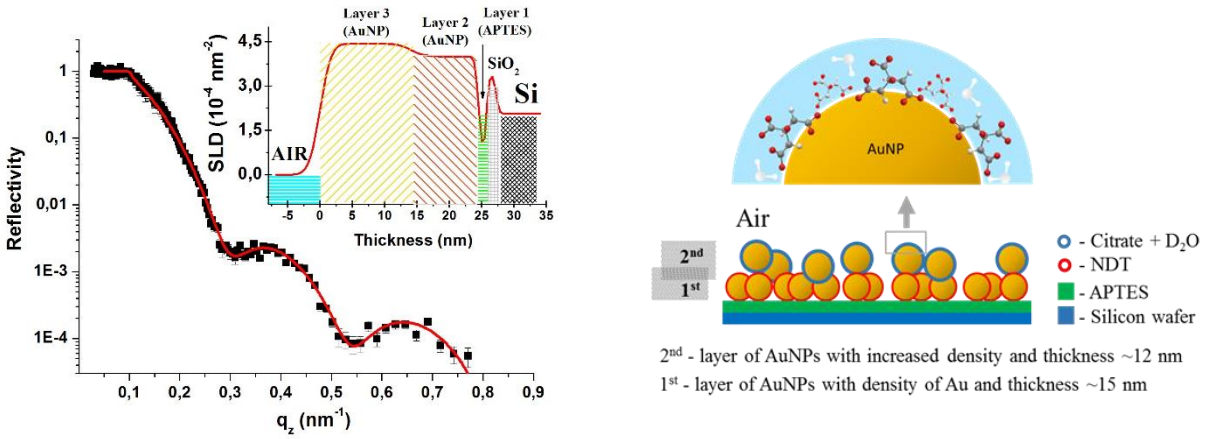

a) *b)*

Fig. I-1-5. *Layers of functionalized gold nanoparticles on silicon substrate: neutron reflectometry data with the corresponding SLD profile and a model suggested for structural organization of gold particles on the surface.*

In the framework of the studies of aqueous magnetic fluids for biomedical purposes, combined experiments on small-angle neutron scattering and synchrotron radiation were performed for nanoparticles of various compositions in dry powders and in a liquid carrier [6,7]. The structural peculiarities of the systems with nanoparticles of magnetite, cobalt ferrite, and composite magnetite/cobalt ferrite nanoparticles with a core-shell structure were determined and analyzed. A

specific feature of the systems under study is the use of biocompatible surfactants (including polysorbate-80, polyethylene glycol, etc.) in the stabilizing coating of magnetic particles. The experiments were conducted on the YuMO small-angle scattering spectrometer at the IBR-2 reactor of JINR (Dubna, Russia), as well as on the DIKSI small-angle scattering station at the synchrotron source of the NRC "Kurchatov Institute" (Moscow, Russia). The study was performed in cooperation with the Vernadsky Institute of General and Inorganic Chemistry NASU (Kiev, Ukraine) and the Faculty of Physics of Taras Shevchenko National University of Kyiv (Kiev, Ukraine).

Investigation of carbon nanomaterials

In the framework of research of biological activity of fullerenes, the effects of inhibition and depolymerization of amyloid fibrils (lysozyme, insulin) in aqueous solutions of C60 and C70 fullerenes (synthesized by various methods) were considered [8,9]. The approach combining the analysis of small-angle neutron scattering (YuMO spectrometer), atomic force microscopy and Thioflavin T fluorescence was applied. Thus, out of the two types of solutions under study (solutions prepared by solvent replacement and dilute solutions based on N-methylpyrrolidone (NMP)), C60 and C70 solutions prepared using NMP exhibited a noticeable inhibitory and depolymerizing activity (**Fig. I-1-6**). In order to exclude the effect of a moderately toxic NMP solvent on amyloids, additional experiments were performed with a pure solvent containing the same fullerene amount as in the mixtures. The results of these experiments revealed no effect of the solvent on amyloids. Thus, the residual concentration of the primary NMP solvent in aqueous solutions of fullerenes is not the cause of the effects of depolymerization/inhibition of amyloid fibrilization. The analysis of the small-angle scattering data revealed several stages of amyloid depolymerization. The study was performed in cooperation with the Institute of Experimental Physics of the Slovak Academy of Sciences (Košice, Slovakia) and the Faculty of Physics of Taras Shevchenko National University of Kyiv (Kiev, Ukraine).

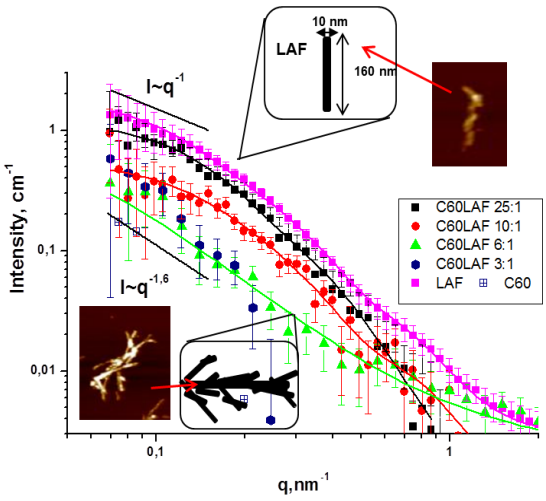

Fig. I-1-6. SANS data for mixtures of amyloid fibrils of lysozyme with aqueous fullerene solution NMP/nC60 in different proportions.

In the framework of the study of kinetic effects in fullerene solutions, a method was suggested for calculating the evolution of the size distribution functions of C60 fullerene clusters in polar solvents [10, 11]. This method makes it possible to calculate the distribution function f(r,t) at

an arbitrary point of time for any given system parameters (**Fig. I-1-7**). A theoretical description of the critical effect of dilution of polar solutions of C60 fullerene with water was proposed as well. This effect (found experimentally in the solutions of C60 in N-methylpyrrolidone) consists in an abrupt decrease in the fullerene aggregate size when the volume fraction of added water exceeds ~ 40%.

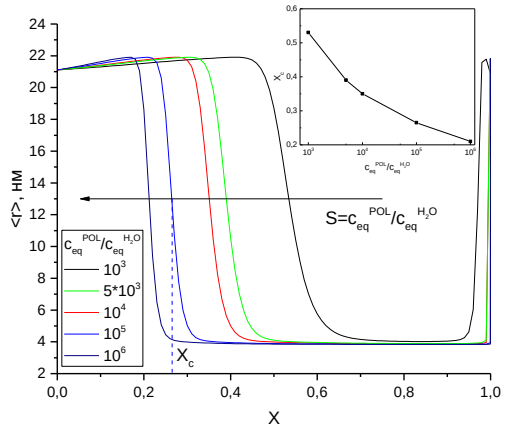

Fig. I-1-7. Dependence of the average cluster size in the C60/NMP solution after dilution with water at the time t = 1 on the degree of dilution, X, for different values of the ratio $S = c^{POL}/c^{H2O} = 10^3$, $5*10^3$, 10^4, 10^5, 10^6 (curves from right to left). The inset shows the dependence of the critical value of the dilution factor, X_c, on S.

The effect was explained using a special dependence of saturation concentration of the system, which takes account of solubilization properties of the solvent with respect to fullerenes: $c_{eq}^{MIX} = c_{eq}^{H_2O} 10^{X\left(\lg c_{eq}^{POL} - \lg c_{eq}^{H_2O}\right)}$, where X is the model parameter characterizing the degree of dilution; $c_{eq}^{H_2O}$ is the equilibrium concentration of complexes in water; and c_{eq}^{POL} is the equilibrium concentration of complexes in a polar solvent.

Investigation of layered nanostructures and electrochemical interfaces

In the framework of structural studies of electrochemical interfaces [12], neutron reflectometry experiments (GRAINS reflectometer) were conducted on model planar systems 'solid electrode-liquid electrolyte' with changing contrast between the electrode and electrolyte [13]. We tested specialized cells that allow experiments with anhydrous electrolytes based on organic solvents, which are actively used today in lithium-ion batteries and supercapacitors. The sensitivity of neutron reflectometry (implemented on a time-of-flight reflectometer at the IBR-2 reactor) to the formation of the solid electrolyte interphase (SEI) on the surface of a thin-film metal electrode in in-operando conditions, was studied (**Fig. I-1-8**).

a) ***d-PC***

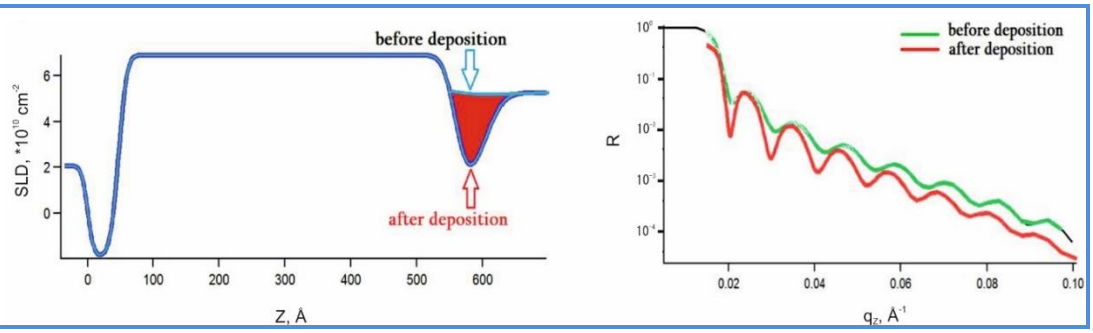

*b) **h-PC***

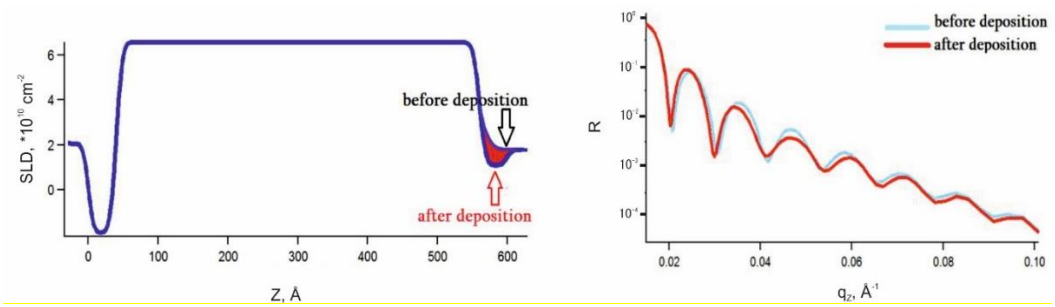

Fig. I-1-8. *Effect of the formation of solid electrolyte interphase (SEI) on the reflectivity curves from the interface of a metal electrode (Cu on Si) in contact with a liquid electrolyte (0.1 M $LiClO_4$ solution in propylene carbonate, PC) based on deuterated (a) and protonated (b) solvents. The obtained scattering-length density (SLD) profiles and corresponding reflectivity curves before and after SEI layer formation.*

The study was performed in cooperation with the Faculty of Chemistry, Moscow State University (Moscow, Russia), Dubna University (Dubna, Russia) and Engineering Incubator Ltd. (Dubna, Russia).

The magnetic states of layered ferromagnetic-superconducting nanostructures Nb(70nm)/Ni(65%)Cu(35%)(7nm)/Si were studied by polarized neutron reflectometry. The dependences of the intensity of specularly reflected neutrons from this structure under various conditions are shown in **Fig. I-1-9a,b**. The black curve corresponds to the magnetic field of 25 Oe, the red one – to the field of 25 Oe, but the system was pre-magnetized in the field of 500 Oe, the blue one – to the field of 200 Oe. As one can see, the state formed at 9 K is also repeated at 4 K.

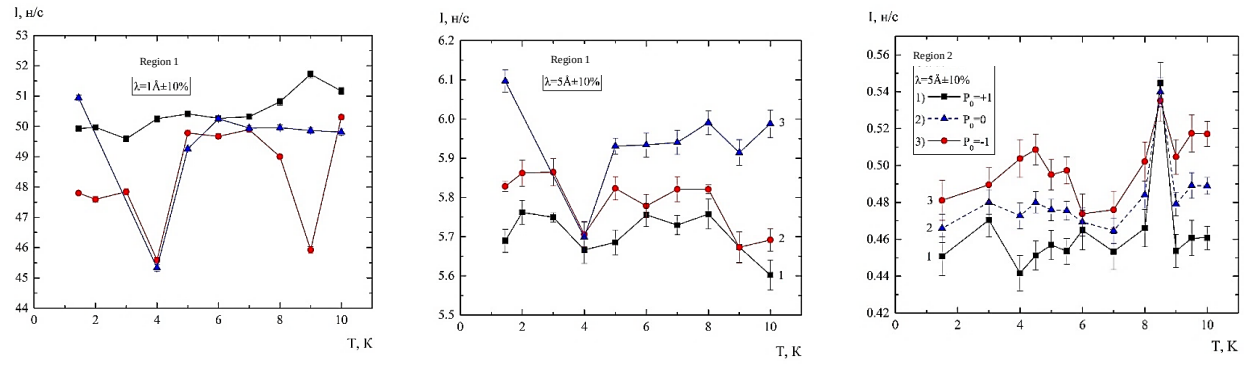

a) *b)* *c)*

Fig. I-1-9. *Intensity of specularly reflected beam from nanostructure Nb(70nm)/Ni(65%)Cu(35%)(7nm)/Si at λ = 1 Å (a) and λ = 5 Å (b). Scattering into the region outside the specularly reflected beam (c).*

The analysis shows that the scattering occurs from a domain lattice structure with interplanar spacing in the range of 0.3-2 nm, which can be identified as cryptoferromagnetic. **Figure I-1-9c** shows the neutron scattered intensity in the region around the specular beam. The scattering occurs from a lattice of clusters with magnetic moments directed against the magnetic field. The lattice spacing is 3.5 nm. It can be seen that the two types of scattering are correlated. It may be suggested that the crypto-state occures in the space between the clusters, where the external field is compensated by the field scattered from the clusters.

To explain the reversibility of magnetic lattice formation, two models were proposed. In the first model, at T ≈ Tc the structures are formed due to the proximity effect when the superconductor is in contact with the surface layer of a ferromagnet. At T = 4 K the entire ferromagnetic layer becomes superconducting. In the second model, the wave vector of the superconducting pair (proportional to the energy of the exchange interaction of localized magnetic moments with the pair) meets the conditions kf(Tc) df=2π, kf(4K) df=4π. As a result, when the pair passes through the ferromagnetic layer, due to the interference of pair reflections from the boundaries of the ferromagnetic layer, equal conditions for the crypto-state are created.

Investigation of biological nanosystems, lipid membranes and lipid complexes

The supramolecular organization of visual pigment rhodopsin in the photoreceptor membrane was studied by small-angle neutron scattering with contrast variation. Visual pigment rhodopsin is a typical representative of a large family of G-protein-coupled receptors (GPCRs). GPCRs function in the dimeric or oligomeric states in membranes. However, the functional role of the dimeric state of rhodopsin and the whole class A of rhodopsin-like GPCRs has not yet been established. The supramolecular organization of rhodopsin in photoreceptor membranes is currently the subject of contentious debates. For many years, it has been generally accepted that rhodopsin functions in the monomeric state. The standpoint was based on the study of the lateral diffusion of rhodopsin in photoreceptor membranes. At the same time, on the basis of photoreceptor membrane images obtained using atomic force microscopy, it was suggested that rhodopsin molecules in this membrane have a dimeric organization. The investigation of the crystal structure of the deprotonated form of photoactivated rhodopsin also revealed its dimeric state, which led to the conclusion that the rhodopsin dimer is a functional unit. Recently, however, a number of papers have been published that support the original idea of the supramolecular organization of rhodopsin as a monomer in photoreceptor membranes. The samples under study were 'disk' membranes with rhodopsin isolated from fragments of rods, as well as rod fragments themselves. On the basis of the results of the experiments on small-angle neutron scattering with contrast variation (YuMO spectrometer, IBR-2) and small-angle X-ray scattering (Rigaku spectrometer, MIPT, Dolgoprudny, Russia and BM-29 BioSAXS facility, ESRF, Grenoble, France), layered structures with the dimensions corresponding to the transverse dimension of the disks were revealed in the rod fragments. It was also shown that rhodopsin is uniformly distributed in the membrane, as in the case of the samples of "disks" isolated from the rod fragments.

Small-angle neutron scattering was used to determine the structural organization of nanodrug doxolip (**Fig. I-1-10**). Doxolip (doxorubicin embedded in the lipid bilayer of soybean phospholipids) is a critically small vesicle. The structure of doxolip is stable with respect to its concentration in water (5-25%) and temperature variation (20-37°C).

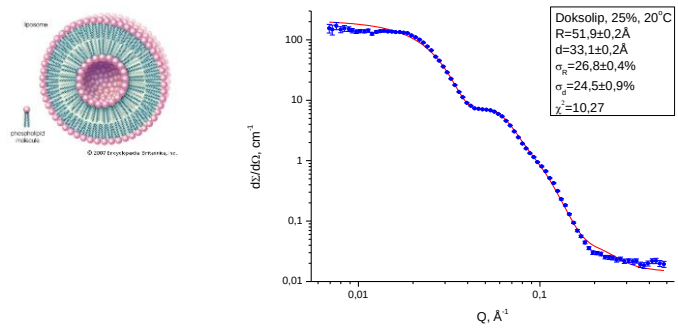

Fig. I-1-10. *Structural model and small-angle scattering curve of doxolip.*

Polymeric materials

Neutron reflectivity curves (GRAINS reflectometer) for thin-film polymer nanocomposites based on polystyrene (or its deuterated analogue) with an addition of C_{60} and C_{70} fullerenes were obtained. Simultaneously with neutron experiments, the samples were studied using atomic force microscopy in cooperation with FLNR JINR (A. Oleinichak). Since the literature data on the organization of fullerene C_{60} in thin polystyrene films are controversal, for the first-time investigations were extended to include systems with fullerene C_{70}. The temperature dependence of reflectivity curves of nanocomposite films with fullerene C_{60} in the vicinity of the glass transition temperature was obtained and analyzed. The approximations of the curves when determining the scattering length density profile from the reflectometry data were compared for the cases with the absence and presence of an oxide layer on the substrate (float glass) (**Fig. I-1-11**).

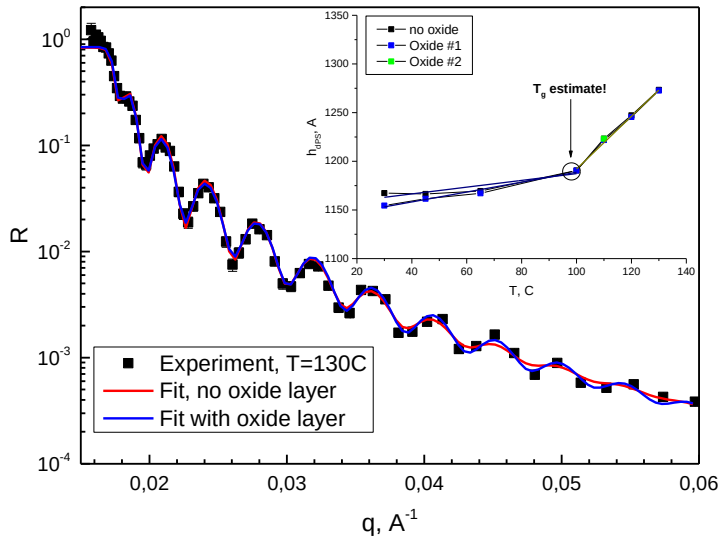

Fig. I-1-11. *Neutron reflectivity curve from dPS/C60 nanocomposite film at T = 130°C. The inset shows the temperature dependence of film thickness obtained from reflectometry data; the break in the dependence corresponds to the glass transition temperature of the material, T_g.*

It was found that the glass transition temperature of composite films depends strongly on the disperse state of fullerene in the initial solution used in the preparation of the nanocomposite. Thus, the formation of fullerene aggregates in this solution shifts the glass transition temperature of the final system by approximately 10°C towards higher values. At present, the possibilities are considered of applying the latest developments in the theory of glass transition of polymers [14, 15] to composites.

In a series of experiments on small-angle neutron scattering performed on YuMO (Dubna, Russia), MAUD (Řež, Czech Republic), KWS-3 (Garching, Germany), the formation of silicate (silicon dioxide) clusters in water-alcohol solutions of tetraethoxysilane (TEOS), $Si(OC_2H_5)_4$, was studied. The cluster formation was initiated by sol-gel polymerization of TEOS under alkaline conditions (pH ~ 10.5). To clarify the structural aspects of two-stage clusterization (first, -SiOH functional groups are generated by hydrolysis of alkoxide groups, then these groups undergo condensation to form a silicate polymer through the formation of Si-O-Si bonds), the contrast variation method was applied with a change in the fraction of the deuterated component in both water and alcohol fractions of the initial solution [16]. Two types of experiments for different molar ratios of H_2O/TEOS in the solution showed (**Fig. I-1-12**) that the cluster structure contains neither residual hydroxyl groups nor unhydrolyzed alcohol groups. This result contradicts theoretical models which employ the idea of unhydrolyzed ("poisoned") alcohol groups to explain the dependence of the cluster structure on the H_2O/TEOS ratio. Apparently, there is a large

conformational variety of polymeric structures (formed from hydrolyzed tetraethoxysilane in alkaline solutions) which are sensitive to the hydrolysis rate determined by the amount of water in the solution. The study was performed in collaboration with the Faculty of Physics of Taras Shevchenko National University of Kyiv (Kiev, Ukraine).

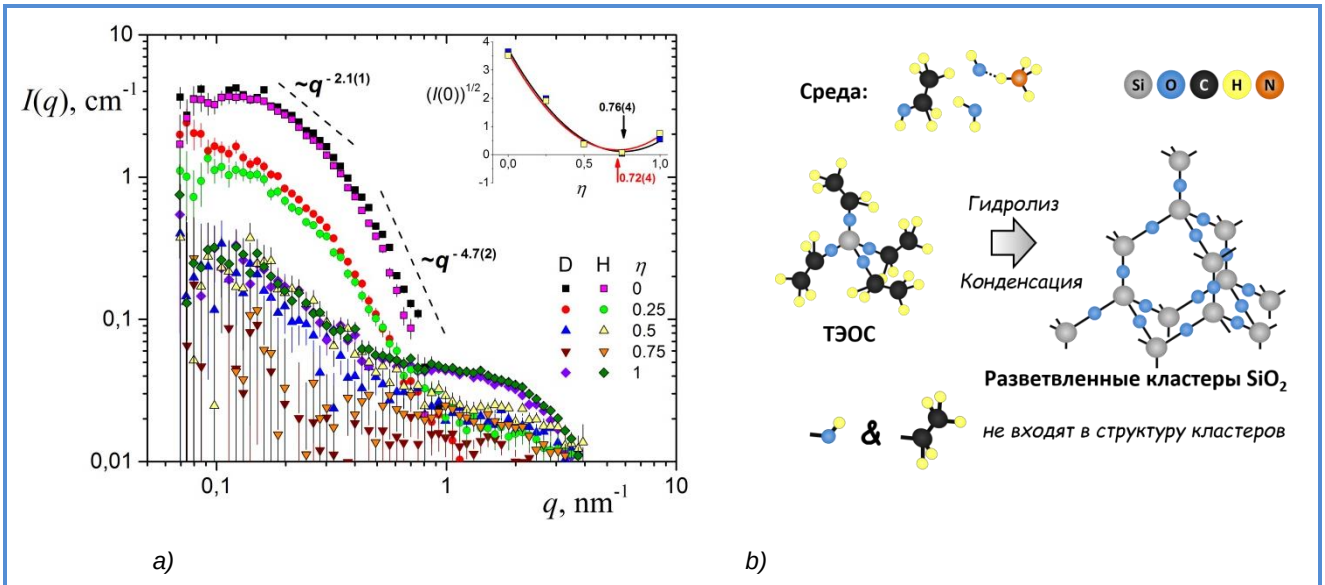

a) *b)*

Fig. I-1-12. *(a) Contrast variation in the SANS experiments on two (light and heavy water) types of water-alcohol solutions of silicate clusters of hydrolyzed TEOS. The inset shows the experimentally obtained values of forward scattered intensity, $I(0)^{1/2}$, as a function of volume fraction of D-ethanol, η, together with parabolic approximations and corresponding match points. (b) Molecular models of the components of the initial solution and those obtained in the course of hydrolysis/condensation of silicon dioxide clusters.*

In the framework of the studies of mixed solutions of polymers and surfactants, the effect of polymers (polyethylene glycol) on the formation of micellar aggregates of sodium oleate [17] and dodecylbenzenesulfonic acid [18] was considered. This study was aimed at clarifying the equilibrium structural features of aqueous magnetic fluids for biomedical purposes, where one of the surfactants under study (sodium oleate) is used as a stabilizer of magnetic particles, and the polymer is added to enhance the biocompatibility of the system. Small-angle neutron scattering (SANS) was used to determine the structural parameters of micelles in solutions with different surfactant concentrations in the absence and presence of polyethylene glycol. The results of the SANS analysis were complemented by the experiments on the measurement of surface tension to determine the surface properties of mixed solutions. A number of qualitative changes in the behavior of micelle parameters (aggregation number, mean radius, degree of ionization, anisotropy, surface potential) were detected when increasing the surfactant concentration for different surfactant/polymer ratios, which is indicative of the interaction of polymer chains with micelles. The study was performed in collaboration with the Wigner Research Center for Physics of the Hungarian Academy of Sciences (Budapest, Hungary) and the Faculty of Physics of Taras Shevchenko National University of Kyiv (Kiev, Ukraine).

Atomic and molecular dynamics

Organic conjugates of the donor-acceptor type that can be used as synthons of specific molecular configurations in the crystal structure are of current interest in the field of structural design of new functional materials for electronic technologies. The structure and dynamics of molecular complexes of bromoaniline and chloroanilinic acids (BrA and ClA) with picolines (2-MP, 3-MP) were studied, **Fig. I-1-13** [19]. From X-ray diffraction experiments on single crystals at T = 100 K, it was found that in the systems under study the synthons of types B:XA:XA:B, :(B:XA:B):XA, and B:XA:B, where XA and B correspond to molecular groups of acids and picolines, respectively, are formed.

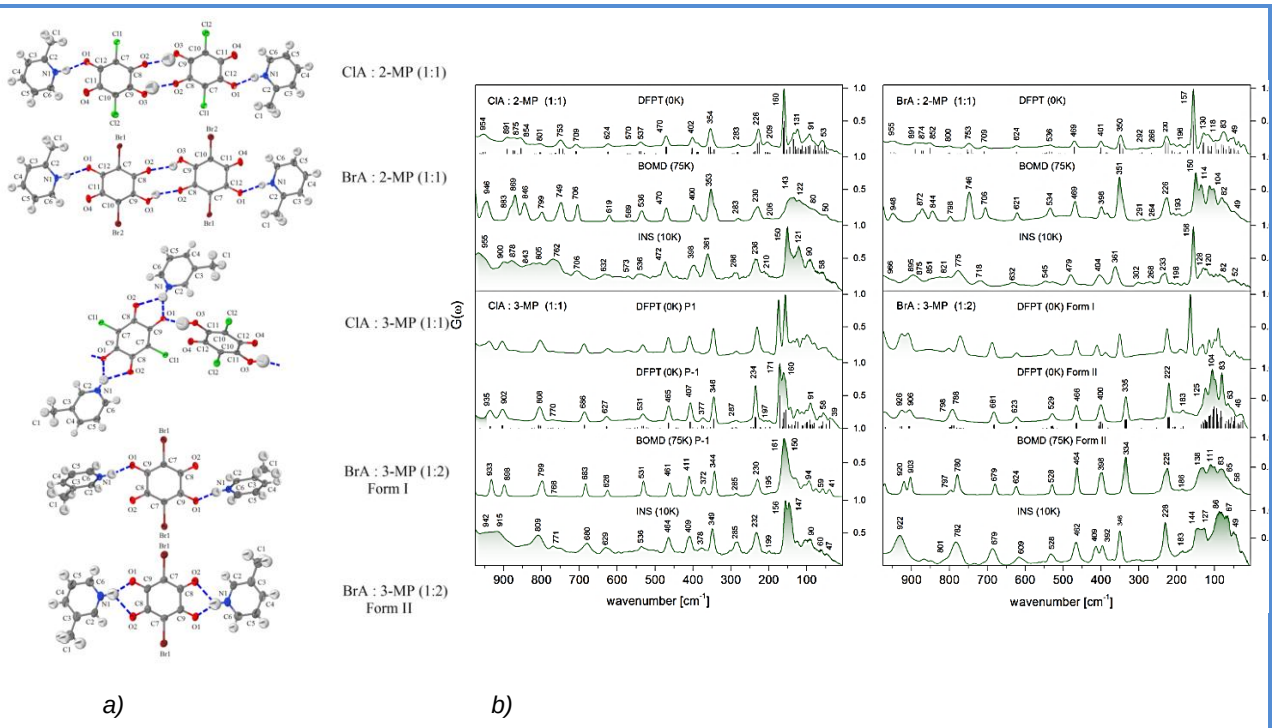

Fig. I-1-13. Structure of molecular complexes of bromoaniline and chloroanilinoic acids with picolines according to X-ray diffraction data (a). Experimental spectra of inelastic neutron scattering from complexes under study and results of theoretical DFPT calculations (b).

The structural studies were complemented by investigations of vibrational dynamics of molecular groups by NMR, optical and neutron spectroscopy and other methods. To analyze the experimental data, we performed theoretical calculations within the DFPT approximation. The role of structural aspects, intermolecular forces, proton transfer, dipole interactions in the formation of the observed spectral features was analyzed.

The vibrational dynamics of glass-forming polar alcohols with a single phenyl ring and inclusions of fluorine atoms (2TFMP, 4TFMP and BEP) in glass (obtained from isotropic liquid) and ordered crystalline (obtained by cold crystallization of a metastable supercooled state) states was studied by incoherent inelastic neutron scattering and infrared spectroscopy, **Fig. I-1-14** [20]. It was shown that the strength of hydrogen bonds in fluorinated materials is approximately the same. This means that the functional group CF_3 has no profound effect on intermolecular interactions, while

sterical conditions are of importance, especially in the formation of the cluster structure closely related to the changes in the dynamics of fluorinated compounds.

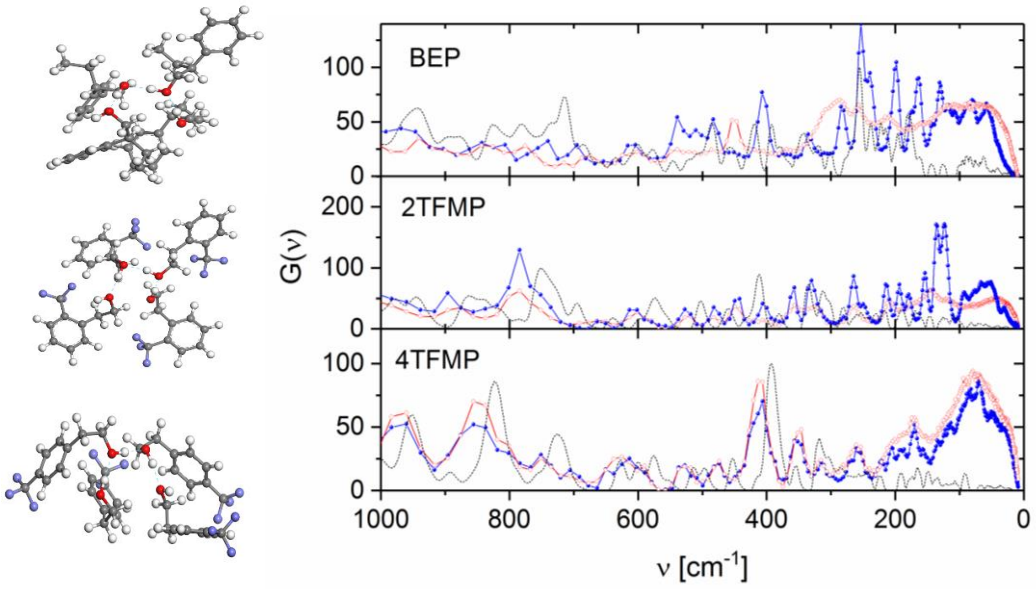

Fig. I-1-14. *Structure of molecular groups (left) and generalized vibrational density of states (right) in solid phases of crystalline state (blue) and glass state (red) at T = 5 K for BEP, 2TFMP and 4TFMP. Dashed lines show the results of theoretical calculations for tetrameric clusters.*

Temperature studies of vibrational modes revealed the important role of hydrogen bonds in molecular interactions. In fluorinated compounds, splitting or asymmetry of the OH stretching mode is observed in the low-temperature region, which demonstrates the existence of different configurations of frozen molecular clusters. Theoretical DFT calculations for tetrameric molecular clusters are in good agreement with the experimental data. When comparing the generalized vibrational density of states of the ordered crystalline phase and the glass phase obtained from an isotropic liquid, one can notice some broadening of the vibrational modes associated with the rotational and translational molecular disorder frozen in the glass state (**Fig. I-1-14**). The difference in the region below 40 cm^{-1} is indicative of the existence of excitations in the glass phase of localized and anharmonic character, which differ from collective phonon excitations propagating in the crystal with a long-range molecular order. The low-energy barrier for torsional motions of CH3-CH2-CH- and OH-C2-CH functional groups connected to the phenyl ring is also observed in the spectra of inelastic neutron scattering in the region of lattice vibrations. The study was performed by the group from Institute of Nuclear Physics Polish Academy of Sciences (Krakow, Poland).

Applied research

At the FSD diffractometer, studies of mechanical properties and basic microstructure parameters of TRIP-composites with austenite matrix and strengthening phase of partially stabilized zirconium dioxide ZrO_2 were continued (**Fig. I-1-15**) in collaboration with the Institute of Metal Forming (Freiberg University of Mining and Technology, Germany). The advantage of these

materials is the ability of both composite components to undergo significant plastic deformations without destruction due to related martensitic transformation mechanisms (TRIP-effect). The purpose of this work was to investigate the effect of plastic deformation on the properties of a new powder composite TRIP-material based on the patented high-alloy austenitic steel and partially stabilized zirconium dioxide ZrO_2. Both structural components have a potential for phase transformation under external stresses. For neutron experiments, a series of TRIP-composites with austenite matrix and strengthening phase of zirconium dioxide ZrO_2 partially stabilized by yttrium oxide (Y-PSZ, series 2) were fabricated by powder metallurgy using hot pressing. In each series, the content of the ceramic phase ZrO_2 was 0, 10, 20, 30, and 100 wt%.

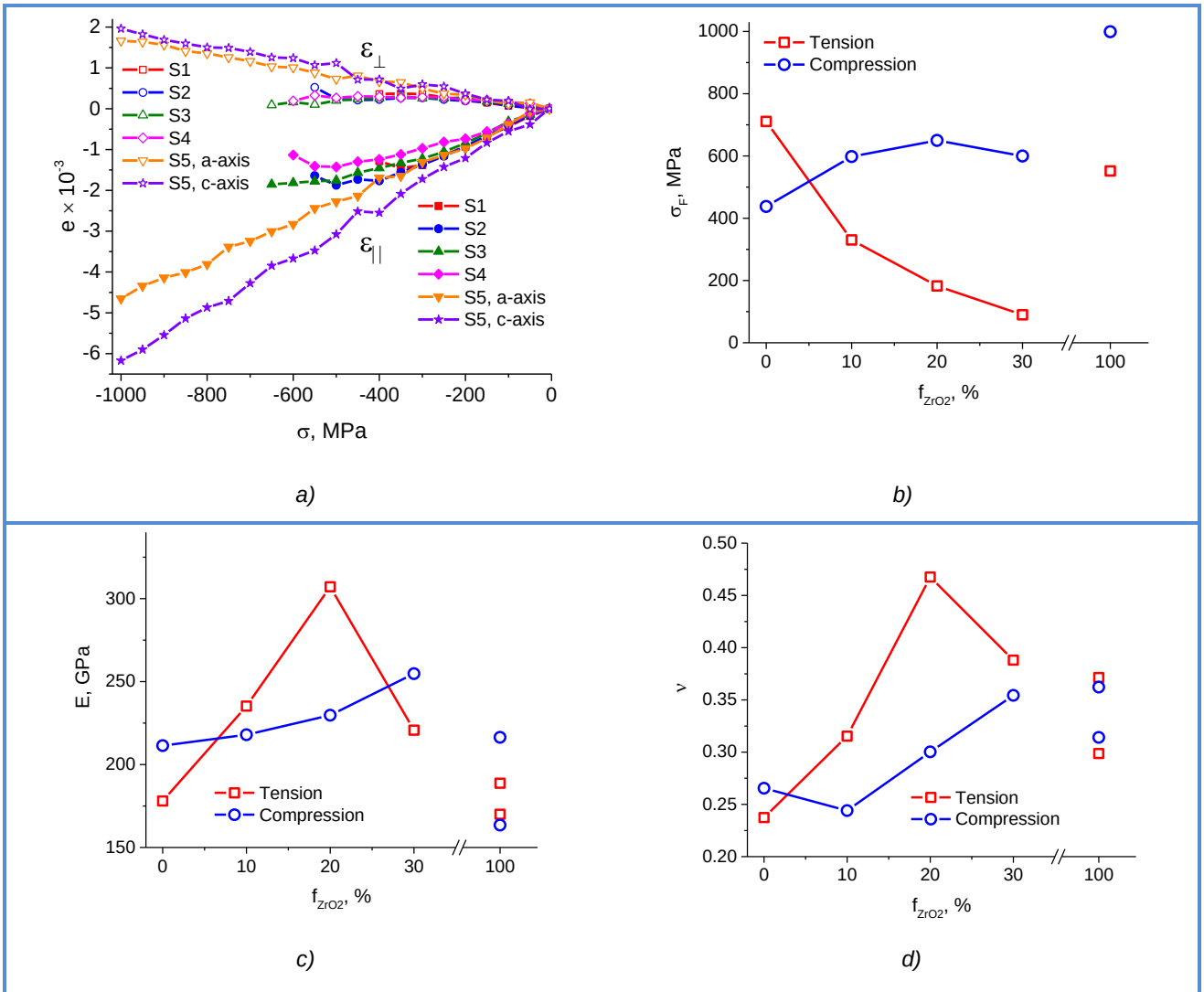

Fig. I-1-15. *a) Deformation curves ε(σ) for austenite matrix of samples S1-S4 and sample S5. Ultimate strength of TRIP-composite (b), Young's modulus (c) and Poisson's ratio (d) for austenite phase in the matrix and sample S5 depending on ZrO_2 content.*

The process of formation of martensitic phases in sample S1 began at stresses of 350 MPa and higher, while for samples S2-S4 practically no martensite phases were observed. Apparently, the reason for this behavior is the redistribution of stresses between the phases of austenite and ZrO_2

ceramics, as well as the formation of microcracks along interphase boundaries. Consequently, the stress level in the austenite matrix did not reach the values sufficient for phase transformations. In the ceramic sample S5 from pure zirconium dioxide (100% ZrO_2), there was only one tetragonal phase in the entire stress range (up to 1000 MPa); no phase transformations were observed.

The obtained ultimate strength values of the material depend on the ZrO_2 content. In addition, there is a significant difference in the strength properties of the material under compression and stretching. The Young's moduli and Poisson's coefficients determined in the elastic region from the linear dependences of ε(σ) also depend on the content of zirconium dioxide and, in addition, significantly differ in magnitude for compression and stretching. Apparently, the main factor explaining this behavior of the material is the formation of microcracks along interphase boundaries in the process of deformation. The fracture surface appearance characteristic for brittle fracture counts in favour of this assumption. In addition, it is confirmed by small stress jumps due to microcracking observed in the deformation curves ε(σ). The microcracks are most likely localized on the residual pores of the ceramic phase, which results in further elastic deformation of the composite.

In collaboration with MEPhI, first experiments on physical and mechanical destruction tests of steel X18H10T were conducted. The data of two methods (scanning contact potentiometry and thermal neutron diffraction) were recorded synchronously (**Fig. I-1-16**). In the course of the experiment, the sample was subjected to an external uniaxial tensile stress in the range of 100 ÷ 750 MPa *in situ* in a neutron beam using an LM-29 testing machine. At stresses above 400 MPa, the deformation of the material was of a plastic nature and manifested itself in a noticeable broadening of diffraction peaks due to an increase in the dislocation density in the material. In addition, the formation of α'-martensite phase was observed in the austenite matrix in the region of plastic deformations at stress rates higher than 650 MPa. At applied stresses above 700 MPa, the formation of a neck in the right part of the specimen was visually observed, which pointed to the localization of plastic deformation in this region and the termination of plastic deformation in the remaining volume of the sample.

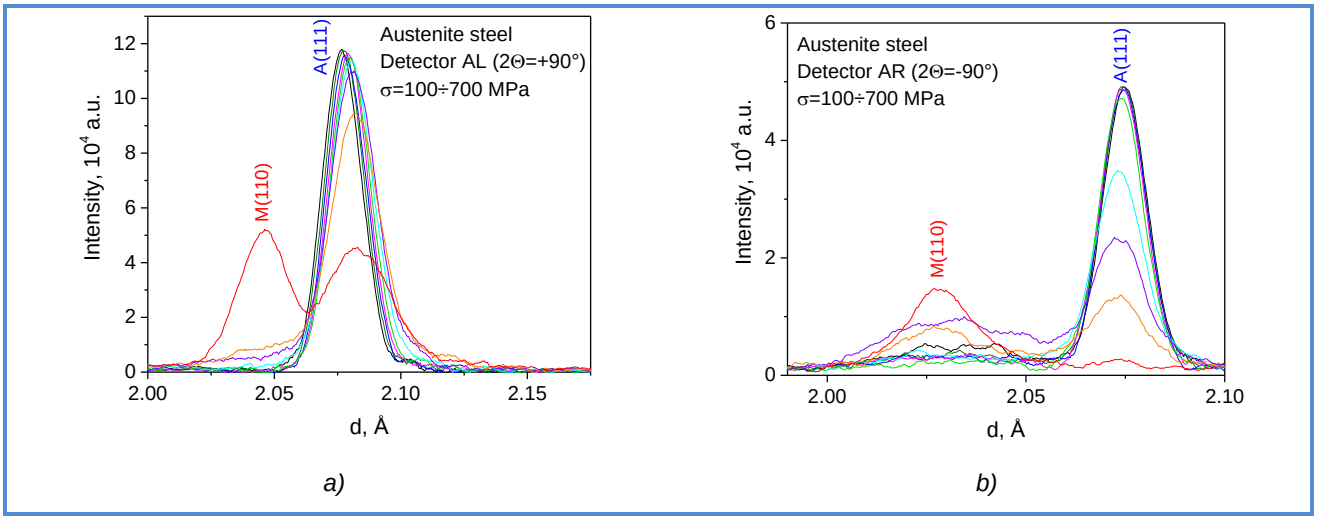

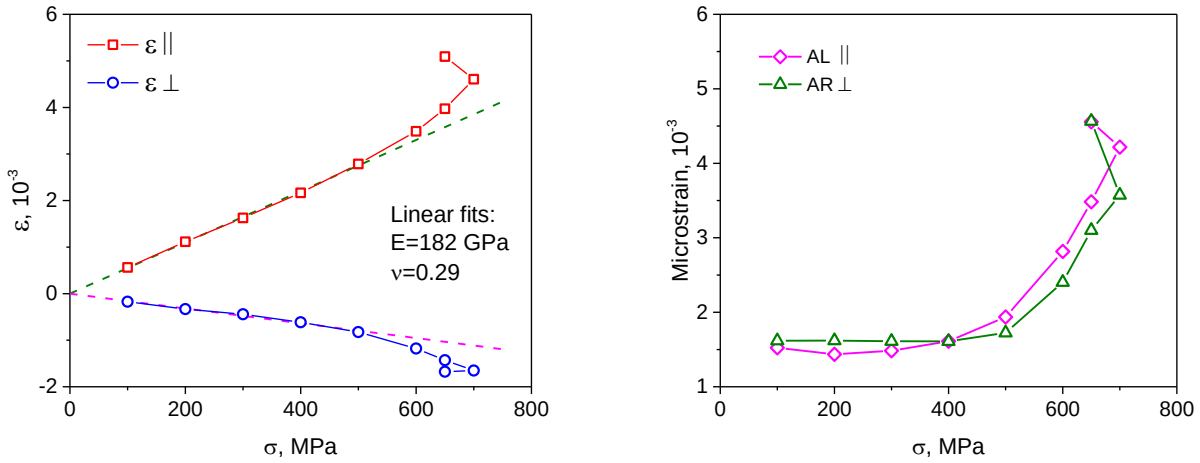

Fig. I-1-16. *Evolution of diffraction spectra measured by 90°-detectors AL and AR, in the region of (111) austenite and (110) martensite peaks depending on the applied stress (a,b). Deformations of the crystal lattice for the austenite phase (c). From the linear approximation of the data in the elastic region (up to 400 MPa), estimates were made for the elastic modulus and Poisson's ratio for the austenite phase: E = 182 GPa, v = 0.29. Microdeformation averaged over all (hkl) as a function of the applied stress (d).*

Potentiometric measurements were performed using a desktop device *Spectroelph-FRR*, intended for spectral analysis of electrical signals. To study the deformation activity of the surface and surface strain waves formed during sample stretching, the time-frequency analysis technique was used. Spectrograms were obtained for all stresses, giving the value for the signal energy in the time-frequency neighborhood of the selected point. The preliminary analysis of the maps of surface potentiograms showed that at low stresses a slight increase in the signal intensity in the potentiograms begins at the center of the sample, and at stresses above 300 MPa the intensity grows significantly and becomes localized at the right part of the sample at the neck formation site at the end of mechanical tests. Further analysis of data aims at finding the relation between the crystal lattice deformation and deformation activity of the surface electrical potential, as well as detecting signs of formation and growth of fatigue embryonic cracks.

The metal-matrix composite Al/SiCp (17% SiC) subjected to thermal treatment was studied by neutron diffraction. On the basis of three isolated diffraction peaks from the SiC phase and four peaks from the Al-phase, lattice deformations were determined and compared with those calculated in the framework of the elastoplastic model, which made it possible to find the parameters determining the plastic deformation of the Al matrix (critical permissible shear stress and hardening parameter). Taking into account previous studies, it was shown that after elastic-plastic deformation, the mismatch in both phases decreases during plastic deformation. The approach combining diffraction experiments and self-consistent calculations was used to study the mechanical behavior of grain groups in stainless duplex steel and Al/SiC composites. Particular attention was paid to the role of second-order stresses in the stresses of phase fluidity, as well as the evolution of these stresses during the plastic process. The intercrystalline stresses were determined from lattice deformations measured *in situ* during the tensile tests. Diffraction

experiments were performed at a synchrotron (ID15B, ESRF, Grenoble, France) and neutron TOF-diffractometer (EPSILON, FLNP JINR, Dubna) [21].

The SKAT diffractometer was used to study the texture of quartz rocks from the Adula Nappe region in the Central Alps (Switzerland) which comprises pre-Mesozoic basement and minor Mesozoic sediments that underwent Paleogene eclogite-facies metamorphism. In the north, the Adula Nappe ends with a blade with a complex internal structure containing the Val-Scaradra shear zone with steeply dipping foliation. The texture analysis of the quartz rocks revealed the mechanisms of deformation processes occurring in the shear zone, **Fig. I-1-17** [22].

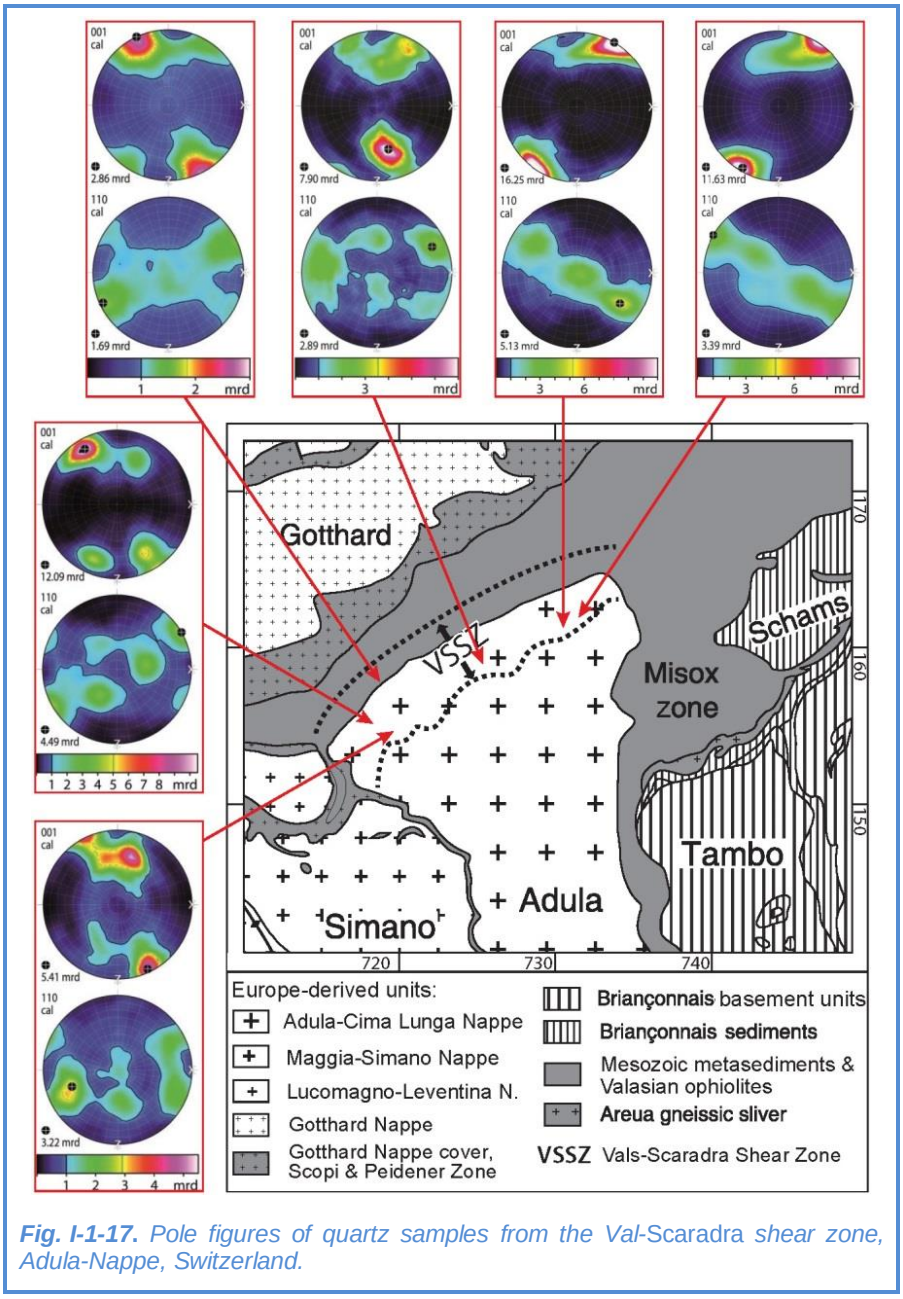

Fig. I-1-17. *Pole figures of quartz samples from the Val-Scaradra shear zone, Adula-Nappe, Switzerland.*

Methods for estimating residual austenite and cementite in high-strength steels using neutron diffraction were developed [23]. Measurements of neutron diffraction spectra were performed on the SKAT texture diffractometer at FLNP JINR in order to exclude the influence of texture on the result. Measurements of calibration samples with the known content of austenite and cementite were made. On the basis of these measurements, calibration lines were constructed and used to determine the proportion of residual austenite and cementite in samples of medium-carbon steels (from 0.3 to 0.4%) with yield strength of 1500 MPa and 1700 MPa after treatment with different annealing temperatures (from 150 to 400°C) and quenching. The results agree well with dilatometry data. In addition, the methods for determining residual austenite and cementite were used for a number of other steels.

The texture in samples of concrete intended for radioactive waste utilization in storage facilities was studied. To obtain a better signal-to-background ratio, measurements were made for samples prepared with heavy water. For a sample with sand, 1368 diffraction spectra were obtained and corresponding pole figures (10-11) and (11-20) were plotted on a 5˚ × 5˚ grid for the SiO_2 phase. The summed spectra measured with an interval of one year for two samples of different chemical composition were compared. The measurements were carried out under the same conditions. It was revealed that for one of the samples the background drastically increased, which is probably due to the high porosity and absorption of moisture from the surrounding atmosphere. For another sample, this effect was not observed, but in both samples the crystallization processes continue. It is planned to continue these studies for samples of other chemical composition and samples subjected to external stresses.

The crystallographic texture of shells of bivalve mollusks was studied. It was revealed that the texture of the calcite phase is very sharp for the mollusk species of Mytilus galloprovincialis, Mytilus trossulus, Mytilus edulis. The crystallographic texture of bivalve mollusk shells has a different character for different phases (calcite, aragonite). A hypothesis was proposed suggesting that the crystallographic texture for species of the same genus is very similar and different for species belonging to different classes. To confirm this hypothesis, new measurements are planned for shells of bivalve mollusks of other species.

At the spectrometer of neutron radiography and tomography, studies of objects of cultural heritage were continued. Thus, a Viking fibula was studied, for which a 3D model of the internal structure based on tomographic data was reconstructed (**Fig. I-1-18**).

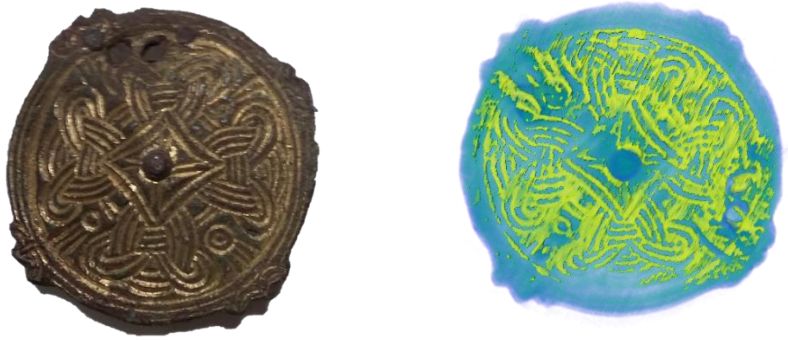

Fig. I-1-18. *Photo (left) and tomographic 3D model of Viking fibula (right).*

The obtained results will allow us to analyze the features of ancient technologies for manufacturing similar objects in Scandinavia.

References

[1] D.P.Kozlenko, K.Drużbicki, S.E.Kichanov, E.V.Lukin, H.-P.Liermann, K.V.Glazyrin, and B.N. Savenko “Anomalous lattice compression and magnetic ordering in CuO at high pressures: a structural study and first principles calculations”, Phys. Rev. B, v. 95, p. 054115 (2017).
[2] N.O.Golosova, D.P.Kozlenko, S.E.Kichanov, E.V.Lukin, H.-P.Liermann, K.V. Glazyrin, and B. N. Savenko, “Structural and magnetic properties of Cr_2O_3 at high pressure”, Journal of Alloys and Compounds, v. 722, pp. 593 – 598 (2017).
[3] I.A. Bobrikov, N.Yu. Samoylova, O.Yu. Ivanshina, S.V. Sumnikov, R.N. Vasin, E.A. Korneeva and A.M. Balagurov “Abnormal phase-separated state of $Li_xNi_{0.8}Co_{0.15}Al_{0.05}O_2$ in the first charge: effect of electrode compaction”, submitted to Electrochimica Acta (2017).
[4] A.M. Balagurov, I.A. Bobrikov, J. Pons, J. Cifre, L.Y. Sun, I.S. Golovin “Structure of the Fe-Mn-Si alloys submitted to γ ↔ ε thermocycling”, submitted to Matt. Charact (2017).
[5] Snegir S.V., O.P. Artykulnyi, V.I. Petrenko, M. Krumova, V.Ye. Kutsenko, M.V. Avdeev, L.A. Bulavin, On the structure of assemblies of coated Au nanoparticles on silicon substrate. Applied Nanosciences (2017), submitted.
[6] Nagornyi A.V., Avdeev M.V., Elenich A.V., Solopan S.A., Belous A.G., Shulenina A.V., Turchenko V.A., Solviev D.V., Bulavin L.A., Aksenov V.L., Structural features of composite magnetic nanoparticles $Fe_3O_4/CoFe_2O_4$ by scattering of X-rays and neutrons, Cryst. Rep. (2017), accepted.
[7] Veligzhanin A.A., D.I. Frey, A.V. Shulenina, A.Yu. Gruzinov, Ya.V. Zubavichus, M.V. Avdeev, Characterization of aggregate state of polydisperse ferrofluids: some aspects of anisotropy analysis of 2D SAXS in magnetic field, J. Magn. Magn. Mater. (2017) in press.
[8] Lynchak O.V., Yu I. Prylutskyy, V. K. Rybalchenko, O. A. Kyzyma, D. Soloviov, V. V. Kostjukov, M. P. Evstigneev, U. Ritter and P. Scharff. Comparative Analysis of the Antineoplastic Activity of C60 Fullerene with 5-Fluorouracil and Pyrrole Derivative In Vivo. Nanoscale Research Letters, 2017, 12:8.
[9] Prylutskyy Yu.I., I.V. Vereshchaka, A.V. Maznychenko, N.V. Bulgakova, O.O. Gonchar, O.A. Kyzyma, U. Ritter, P. Scharff, D.M. Nozdrenko, I.V. Mischenko. C60 fullerene as promising therapeutic agent for correcting and preventing skeletal muscle fatigue. J. Nanobiotechnol., 2017, 15:8.
[10] Tropin T.V., Avdeev M.V., Aksenov V.L., Modelling of evolution of cluster size distribution functions in polar solutions of fullerene C60, Cryst. Rep. (2017), in press.
[11] Tropin T.V., Aksenov V.L., Theoretical studies of the effect of dilution of fullreren polar solutions by water, JETP Letters (2017), submitted.
[12] Avdeev M. V., Bobrikov I.A., Petrenko V.I., Characterization of Battery Materials: Neutron Methods, In Electrochemical Storage Materials – From Crystallography to Manufacturing Technology, Eds. D.C. Meyer, T. Leisegang, H. Stöcker, De Gruyter: 2017, in press.
[13] Petrenko V.I., I.V. Gapon, A.A. Rulev, E.E. Ushakova, E.Yu. Kataev, L.V. Yashina, D.M. Itkis, M.V. Avdeev, Studies of electrochemical interfaces by TOF neutron reflectometry at the IBR-2 reactor, Journal of Physics: Conf. Series. (2017) accepted.
[14] Tropin T.V., Schmelzer, V.L. Aksenov. On the possibility of modeling of kinetics of glass transition of polymers in a wide range of cooling and heating rates. Journal of Molecular Liquids, 2017, V. 235, pp. 172-177.
[15] Aksenov V.L., Tropin T.V., Schmelzer J.W.P., Kinetic equations for describing glass-liquid transitions in polymers, Theor. Math. Phys. (2017), accepted.
[16] Tomchuk O.V., Avdeev M.V., Bulavin L.A., Ryukhtin V.V., Ivankov O.I., Aksenov V.L., Nagornyi A.V. Study of tetraethoxysilane clusters in basic ethanol/water solutions by SANS contrast variation. Romanian Reports in Physics (2017), accepted.
[17] Artikulnyi A.P., Petrenko V.I., Bulavin L.A., Almasy L., Grigoryeva N.A., Avdeev M.V., Aksenov V.L., Effect of polyethylene glycol on the structure of micelle solutions of sodium oleate in water by small-angle neutron scattering, Cryst. Rep. (2017), accepted.
[18] Artikulnyi A.P., Petrenko V.I., Bulavin L.A., Ivankov O.I., Avdeev M.V., Impact of poly (ethylene glycol) on the structure and interaction parameters of aqueous micellar solutions of anionic surfactant. Romanian Reports in Physics (2017), accepted.
[19] Łuczynska, K.; Drużbicki, K.; Lyczko, K.; Dobrowolski, J.Cz. Structure-Spectra Correlations in Anilate Complexes with Picolines, Crystal Growth & Design, 16 (2016) 6069−6083.
[20] Juszyńska-Gałązka E., Zając W., Saito K, Yamamura Y., and Juruś N, Vibrational Dynamics of Glass Forming: 2-Phenylbutan-1-ol (BEP), 2-(Trifluoromethyl)phenethyl Alcohol (2TFMP) and 4-(Trifluoromethyl)phenethyl Alcohol (4TFMP) in their thermodynamic phases, Phase Trans., in press (2017), https://doi.org/10.1080/01411594.2017.1393813.
[21] Gadalinska, E., Baczmanski, A., Wronski, S., Wróbel, M., Wierzbanowski, K., Lodini, A., Klosek, V., Buslaps, T. & Scheffzuek, Ch.: Neutron and Synchrotron diffraction study of elastoplastic behaviour of Al/SiCp metal matrix composite. Materials Science Forum 905, 66-73 (2017).
[22] Kossak-Glowczewski, J., Froitzheim, N., Nagel, T.J., Pleuger, J., Keppler, R., Leiss, B. & Regent, V., Along-strike shear-sense reversal in the Vals-Scaradra Shear Zone at the front of the Adula Nappe (Central Alps, Switzerland). Swiss J. Geosci. 110 (2), 677-697 (2017).
[23] Lychagina, T., Zisman, A., Yashina, E. & Nikolayev, D. Directly verifiable neutron diffraction technique to determine retained austenite in steel. Adv. Eng. Mater. 1700559 (2017) (doi: 10.1002/adem.201700559).